Detection of Snowmelt Using Spaceborne Microwave Radiometer Data in Eurasia From 1979 to 2007

Matias Takala, Jouni Pulliainen, *Senior Member, IEEE*, Sari J. Metsämäki, and Jarkko T. Koskinen, *Member, IEEE*

***Abstract*—Determining the date of snowmelt clearance is an important issue for hydrological and climate research. Spaceborne radiometers are ideally suited for global snowmelt monitoring. In this paper, four different algorithms are used to determine the snowmelt date from Scanning Multichannel Microwave Radiometer and Special Sensor Microwave/Imager data for a nearly 30-year period. Algorithms are based on thresholding channel differences, on applying neural networks, and on time series analysis. The results are compared with ground-based observations of snow depth and snowmelt status available through the Russian INTAS-SSCONE observation database. Analysis based on Moderate Resolution Imaging Spectroradiometer data indicates that these pointwise observations are applicable as reference data. The obtained error estimates indicate that the algorithm based on time series analysis has the highest performance. Using this algorithm, a time series of the snowmelt from 1979 to 2007 is calculated for the whole Eurasia showing a trend of an earlier snow clearance. The trend is statistically significant. The results agree with earlier research. The novelty here is the demonstration and validation of estimates for a large continental scale (for areas dominated by boreal forests) using extensive reference data sets.**

***Index Terms*—Eurasia, radiometer, Scanning Multichannel Microwave Radiometer (SMMR), snowmelt, Special Sensor Microwave/Imager (SSM/I), time series.**

I. Introduction

SNOW cover and its evolution strongly affect hydrological and climate processes. Snow-covered terrain has an albedo that is considerably higher than that of bare terrain, fundamentally affecting the processes of the atmosphere. Consequently, snow is an important parameter in weather forecasting and climate models (global circulation models and Earth system modeling [1]). Concerning hydrological processes, information on snow depth (SD) or snow water equivalence helps in predicting the water discharge during the melting period [2]. Estimating the timing of snowmelt, either the melting onset or snow clearance, indicates when this takes place, although human activities such as dams and topography also have significant effects to water systems. Satellite data can be used for detecting the snowmelt [3]–[10]. This has also various operational applications. Hydropower plants can better adjust water flow, and authorities can be prepared for possible flood hazards. Melting takes place rapidly, and this is a special challenge for spaceborne snowmelt monitoring. For hydrological applications, snowmelt must be determined in a time scale of one week or even on a daily basis [11]. The timing of the snowmelt is also an important factor for the length of the annual growing season at northern latitudes [12]. As snow melts, the carbon uptake from the atmosphere magnifies [13]. The amount of carbon dioxide in the atmosphere is one of the key factors in global climate change, and thus, the onset and progress of snowmelt provide information that is relevant to annual carbon balance.

A certain amount of heat is needed to initiate the snowmelt. The long-term evolution of the dates of the onset of snowmelt and of snow clearance gives insight whether the snow melts earlier presently than 30 years ago, and thus, information related to global warming is obtained. When the time series of global/large scale maps on the snowmelt are compared (in a statistical manner) with simulations made with existing climate models, the reliability of model predictions can be analyzed.

The time series of global observations on snow cover have been available for three decades from various types of satellite instruments. Passive microwave radiometers have one substantial advantage over optical instruments. Optical instruments observing the Earth's surface, such as spectrometers and scanners, are dependent on the Sun illumination and on cloud-free conditions. Clouds can hinder the use of optical instruments for weeks, which is a critical handicap concerning the mapping of the snowmelt. Microwave instruments, such as multichannel microwave radiometers, do not have this drawback. Additionally, at microwave frequencies, the dielectric constant of water is much larger than that of ice and snow (and majority of natural substances). Thus, the presence of liquid water in a snowpack has a strong effect on microwave emission signatures.

Microwave radiometers have a coarse resolution (on the order of 5–50 km, depending on instrument and frequency) but a wide swath width. For example, the Special Sensor Microwave/Imager (SSM/I) [14] has a swath of 1440 km. Hence, it can measure most of the globe within 24 h. In climate research applications, the coarse spatial resolution is quite acceptable since the resolution of climate models is typically even coarser. For example, the Hadley Centre uses high-resolution regional climate models with a resolution of 50 km $\times$ 50 km and global atmosphere–ocean general circulation models with a resolution of over 100 km [1]. As the resolution of climate models is coarser than that of radiometer data, radiometer-derived products can be used as input and validation data for climate models.

The continuous time series of radiometer data are available starting from 1978. The Scanning Multichannel Microwave Radiometer (SMMR) [15] was launched in 1978 onboard the

Manuscript received September 26, 2008; revised February 2, 2009. First published May 12, 2009; current version published August 28, 2009.

M. Takala, J. Pulliainen, and J. T. Koskinen are with the Finnish Meteorological Institute, 00101 Helsinki, Finland (e-mail: matias.takala@fmi.fi; jouni.pulliainen@fmi.fi; jarkko.koskinen@fmi.fi).

S. J. Metsämäki is with the Geoinformatics and Land Use Division, Finnish Environment Institute, 00251 Helsinki, Finland (e-mail: sari.metsamaki@ymparisto.fi).

Digital Object Identifier 10.1109/TGRS.2009.2018442

Nimbus-7 satellite. It operated until 1987. In 1987, the Defense Meteorological Satellite Program launched its first satellite with the SSM/I onboard. A series of satellites with SSM/I instruments have operated since then, producing nearly continuous stream of data. In 2002, NASA launched the Aqua satellite with the Advanced Scanning Microwave Radiometer onboard.

Algorithms to detect snowmelt from spaceborne microwave radiometer data have been investigated by several authors, typically applying brightness temperatures observed at frequencies of 19 and 37 GHz. The onset of snowmelt in Greenland was investigated by Abdalati and Steffen [3] using a so-called cross-polarized gradient ratio, i.e., $\mathrm{XGPR} = T_{19\mathrm{h}} - T_{37\mathrm{v}} / T_{19\mathrm{h}} + T_{37\mathrm{v}}$, where v and h denote vertical and horizontal polarizations, respectively. Additionally, Hall *et al.* [16] used the cross-polarized gradient ratio for snowmelt detection. A slightly different algorithm was proposed by Drobot and Anderson [4], as they applied the brightness temperature difference $T_{19\mathrm{h}} - T_{37\mathrm{h}}$. Accordingly, Smith [17] employed the brightness temperature difference $T_{19\mathrm{v}} - T_{37\mathrm{v}}$. Takala *et al.* [8] used two channel differences $T_{37\mathrm{v}} - T_{19\mathrm{v}}$ and $T_{37\mathrm{h}} - T_{19\mathrm{v}}$ in a corresponding algorithm for the detection of the onset of snowmelt. Takala *et al.* [8] tested and validated the algorithm for boreal forests (taiga belt) of Finland, whereas Drobot and Anderson [4] and Smith [17] applied their algorithms over the Arctic sea ice.

A time series analysis for snowmelt detection from radiometer data was introduced by Mognard *et al.* [7]. They used channel differences $T_{19\mathrm{h}} - T_{37\mathrm{h}}$ in order to obtain global estimates of the snowmelt for a 20-year period. The results obtained are interesting but lack validation against ground truth. Joshi *et al.* [6] also successfully applied a time series analysis for radiometer observations over Greenland. In this paper, a time-series-based algorithm is introduced for the taiga belt utilizing the channel difference $T_{37\mathrm{v}} - T_{19\mathrm{v}}$.

Artificial neural networks have been used to some extent to map the properties of snow. Tedesco *et al.* [18] applied neural network methods to estimate snow water equivalence and SD. Simpson and McIntire [19] used a feedforward neural network with Advanced Very High Resolution Radiometer data to estimate the properties of snow cover. Takala *et al.* used a self-organizing map (SOM) to estimate the onset of snowmelt with SSM/I data. In this paper, the SOM-based algorithm is modified in such a way that the dependence on knowing snow water equivalence and physical temperature has been eliminated. For comparison, a feedforward neural network is also tested here.

A general problem in earlier work has been the lack of proper ground-truth reference data. In particular, the lack of reference data has been hampering the validation of algorithms for a continent-scale mapping [7] and for periods of several decades [3], [5], [16]. Foster *et al.* [20] have used weather observation and *in situ* radiometer data to validate satellite estimates in tundra, but their work does not cover recent times. Moreover, the work carried out for forested regions has been limited, although the data in [13] and. [7] include forests. The earlier work of the authors of this paper [8], [10] has been focused to boreal forests. In the earlier work, data from the Watershed Simulation and Forecasting System of the Finnish Environment Institute (SYKE) were used as a reference for testing and validating the detection of the onset of snowmelt for the region of Finland. However, the accuracy of model simulations poses a problem. In [9], reference data from the Meteorological Archival and Retrieval System of the European Centre for Medium-Range Weather Forecasts was applied. However, due to the gaps in SD data, referencing had to be performed using surface temperature data. In this paper, extensive Russian INTAS-SSCONE [21] *in situ* SD data covering most of Eurasia are used. This made possible the testing and validation of algorithms covering northern Eurasia for a long time span.

Snow cover and climate changes in Eurasia have been studied extensively using ground-based data, satellite instruments other than microwave radiometers, and physical parameters applying reference information from other than the snowmelt date. Brown [22] has constructed snow cover extent (SCE) and snow water equivalent data from 1915 to 1997 using station data from China, Canada, the U.S., and the former Soviet Union. The results show a reduction of SCE in Eurasia. Serreze *et al.* [23] discuss many physical parameters, which include the snow cover area (SCA) that has been derived using optical satellite data. Their values show below-normal SCA values in the 1990s. Dye [24] has used the last-observed snow cover in spring [week of last snow (WLS)] and other parameters and constructed time series from 1972–2000 using optical satellite observations. His results show three to five days/decade shift in WLS. Bamzai [25] used satellite-derived snow cover data, including snowmelt date, and compared the results to the values of arctic oscillation. His work shows an increase of snow-free days per year. Smith *et al.* [13] have analyzed trends in soil freeze and thaw cycles from 1988 to 2002 using radiometer data. Their results show that soil thaws three to five days/decade earlier, depending on land cover. The results of Foster *et al.* [26] indicate that snow melts four to seven days earlier on Arctic areas since the late 1980s compared to the previous 20 years.

Brown [22] utilizes observations from the station network. This has the advantage of spanning the time series to the beginning of the twentieth century. On the other hand, the spatial and, to some degree, also temporal resolutions are poor. Serreze *et al.* [23], Dye [24], Bamzai [25], and Foster *et al.* [26] use optical data that have excellent resolution but are limited by weather and illumination conditions. Smith *et al.* [13] use microwave radiometer data. They detect the soil freeze and thaw; the latter is a related phenomenon compared to the snowmelt. The time series of Smith *et al.* [13] ended in 2002. This work includes estimates for 2003–2007.

II. Materials and Methods

In this paper, a time series of brightness temperatures covering Eurasia from 1979 to 2007 was used together with INTAS-SSCONE SD and status data. The data are described in detail in Sections II-A and B. Four different algorithms were used to estimate the day of snowmelt. The algorithms are as follows: 1) a channel difference algorithm; 2) a self-organizing neural-network-based algorithm; 3) a feedforward neural-network-based algorithm; and 4) a time series thresholding algorithm. These algorithms are explained in Sections II-C–E.

A. Radiometer Data

A complete time series of radiometer data from 1978 to 2007 has been acquired from the National Snow and Ice Data Center

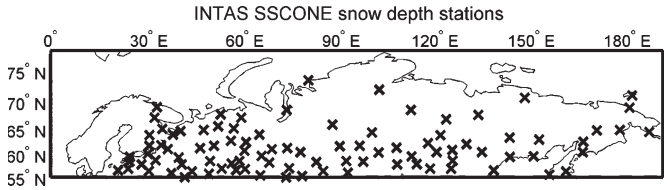

Fig. 1. Locations of SD-measuring stations in INTAS-SSCONE data set.

in Boulder, CO. For the years 1978–1987, the SMMR [15] data from Nimbus 7 are used, whereas for 1987–2007, the SSM/I data from Defense Meteorological Satellite Programs (DMSPs) D-11 and D-13 are used. All data are EASE gridded [14], which means that the projection used is north azimuthal equal area with a nominal resolution of 25 km × 25 km. Geolocation files and exact overpass time (UTC) are provided with the data. For each channel per day, there is a different file for ascending and descending nodes. Since the orbits of DMSP series and Nimbus 7 are Sun synchronous, the local time in every ascending or descending image is the same for all pixels, regardless of the overpass UTC time. The local overpass time varies in time, but the difference between randomly chosen dates is not larger than 2 h. The descending-node image corresponds to early morning (5:00–7:00 A.M. local), while the ascending-node one corresponds to late afternoon (3:00–5:00 P.M. local). In the case of SSM/I, the local time also depends on which DSMP satellite the instrument has been onboard. In this paper, descending and ascending data have been applied separately for each other.

The SMMR has frequencies of 6.6, 10.7, 18.0, 21.0, and 37.0 GHz. At each frequency, vertical and horizontal polarizations are measured, resulting to ten channels. The swath width of the SMMR is about 600 km. The SSM/I has frequencies of 19.3, 22.2, 37.0, and 85.5 GHz. Both horizontal and vertical polarizations are measured, except for 22.2 GHz where vertical polarization is only measured. The swath width is about 1400 km.

The most important frequencies for snow detection are bands around 18 and 37 GHz (available for all instruments). With SSM/I, the footprint sizes are 70 km × 45 km and 38 km × 30 km at 19.3 and 37 GHz, respectively. The SSM/I provides data on a daily basis, and due to the wide swath (1400 km), most of Eurasia can be mapped in 24 h. There are still some data gaps in both time and space. The SMMR had a much more narrow swath (600 km), and thus, averaging over time is a necessity to obtain the necessary areal coverage. The SMMR data are available on every other day only. There are also some long periods when the instrument was switched off.

B. In Situ on Snow Status and Optical Satellite Reference Data

The used reference data are the INTAS-SSCONE SD data set [21] from years 1978–2001. The snowmelt date is estimated from a specific snow status flag included in the data set. Measurements have been made at 223 different locations, as shown in Fig. 1. Depending on the date, some of the data are missing. The worst case is when the data are not available for half of the stations, and the best case is when only ten stations lack observations. There are 1704 and 2205 snow clearance date estimates for the SMMR and SSM/I data with proper validation data, respectively. For each measurement site, there is a WMO station index, date of the measurement, SD in centimeters, a qualitative estimate of the snow-covered area

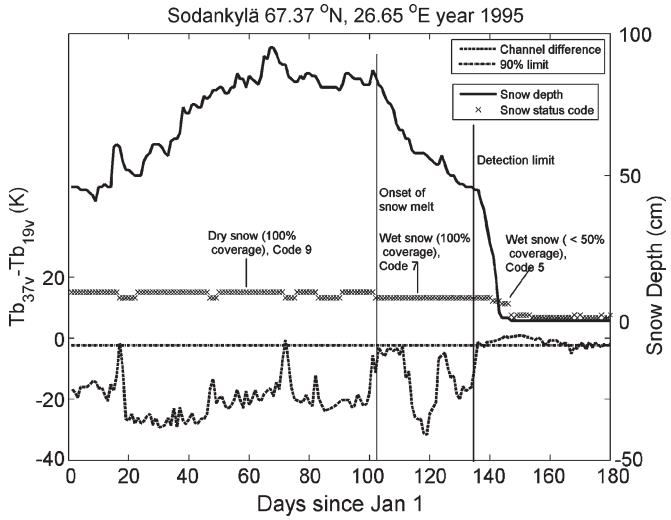

Fig. 2. SD (in centimeters) and snow status codes from FMI weather station data and brightness temperature $T_{37\mathrm{v}} - T_{19\mathrm{v}}$ from SSM/I data [14]. The snow status code has a value of nine for dry snow with 100% coverage and a value of seven for wet snow with 100% coverage. The value of six is wet snow with coverage $> 50\%$, and the value of five is snow with coverage $< 50\%$. The 90% level of difference between the maximum and minimum of the brightness temperature serves as the detection limit.

(SCA), and a status flag value. The flag describes whether the melt is temporary or continuous (snow clearance) and whether the value of SD is correct or to be rejected. The INTAS-SSCONE data set also has a short description of station characteristics, for example, information on whether the station is protected from strong wind or not. As to snowmelt, it is considered to take place if the flag changes from value "SD is correct" to either "temporary melting" or to "continuous melting." If there is more than one such change (typically two to three), only the last one in the 180-day period is taken into account. There are no error estimates in the INTAS-SSCONE data, but in general, the SD measurement can be considered accurate. SD is customarily manually measured with a rod, ensuring reliable data. The automated measurements have also, in general, a proper accuracy. On the other hand, the snowmelt flag is subjective to the observer. Fig. 2 compares the pointwise measurements with satellite-observed brightness temperatures. This demonstrates the correspondence of spatially distributed satellite observations to snow status observations at a single location representing the Eurasian boreal forest belt.

Since the INTAS-SSCONE data embody pointwise observations while the nominal resolution of radiometer data is 25 km × 25 km, it should be investigated whether the INTAS-SSCONE snow flags are suited for validation work considering this discrepancy. We approached this task by investigating the spatial variation of snow cover characteristics within the radiometer resolution cell. Should there be homogenous snow conditions (at least at the time of melting onset or snow clearance when we are most interested at) within the pixel, the upscaling of pointwise measurements to the 25 km × 25 km area is well justified. In the investigation, the optical data provided by the Moderate Resolution Imaging Spectroradiometer (MODIS) was used in order to generate maps describing the fraction of SCA for $0.005^\circ \times 0.005^\circ$ resolution cells (resembling a MODIS nominal resolution of 500 m × 500 m). This was carried out using the SCAmod algorithm by

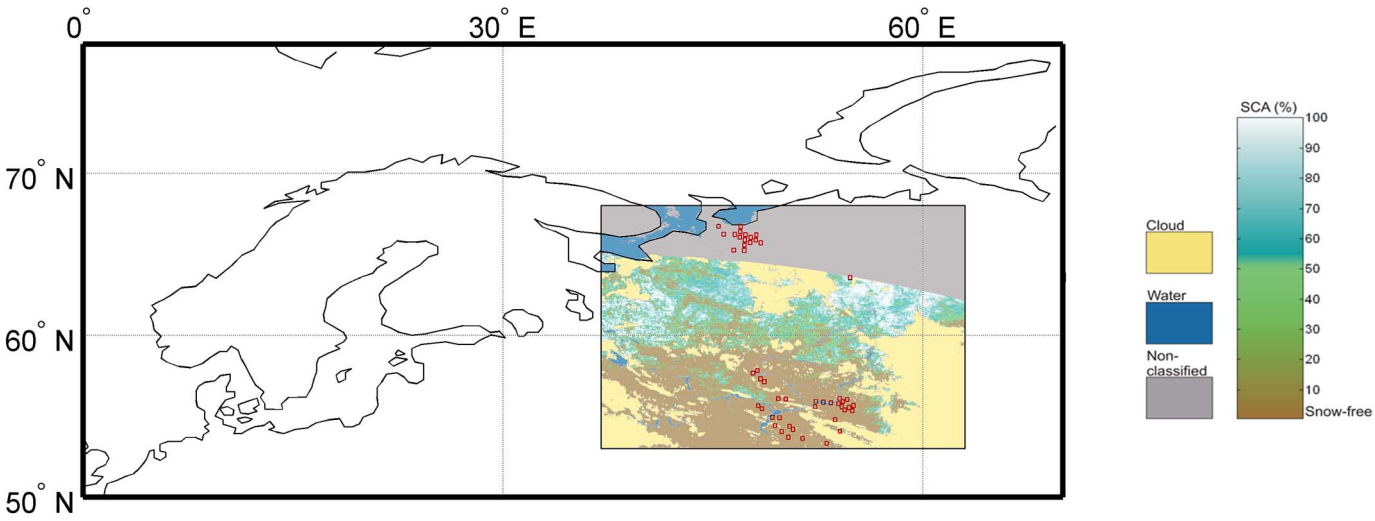

Fig. 3. Example on the MODIS-based SCA map of a large area in Eurasia, also indicating smaller test sites applied for analysis here.

Metsämäki *et al.* [27], which was particularly developed for the boreal zone. As a result, the SCA time series (17 SCA maps) for the snow-melting period of 2001 was obtained for an approximately 1500 km × 1600 km area in northwestern Russia (see Fig. 3). From these maps, 49 subareas corresponding to the size of a radiometer resolution cell were selected for analyzing the spatial variance of SCA at different stages of snow melting. In Fig. 4(a), the evolution of SCAs inside a 25 km × 25 km subarea is presented. The time series include the mean and standard deviation of SCA estimates inside the 25 km × 25 km resolution cell, complemented with individual SCA estimates for 500 m × 500 m sized grid cells.

Fig. 4(a) clearly shows how snow coverage is very evenly distributed at the time of melting onset and snow clearance, while this is not the case during snow melting, e.g., around the average SCA of 40%. The behavior of SCA in the other 48 subareas is very similar to the one shown in Fig. 4(a). This is also shown in Fig. 4(b), where the average standard deviation of SCA as a function of SCA is presented. Clearly, close to the time of snow clearance, the SCA shows very little variation (0.13%). This is evidently due the escalating melting process caused by the gradually increasing proportion of absorptive snow-free ground, again powering the melting of the neighboring snow patches. SD, land cover variability, and other issues are also involved. The analyses show that the difference between snow clearances in the scale of 500 m when compared to the scale of 25 km is typically on the order of ±10 days. This indicates that a pointwise observation of snow clearance can be applied (in a statistical manner) as reference data to radiometer observations.

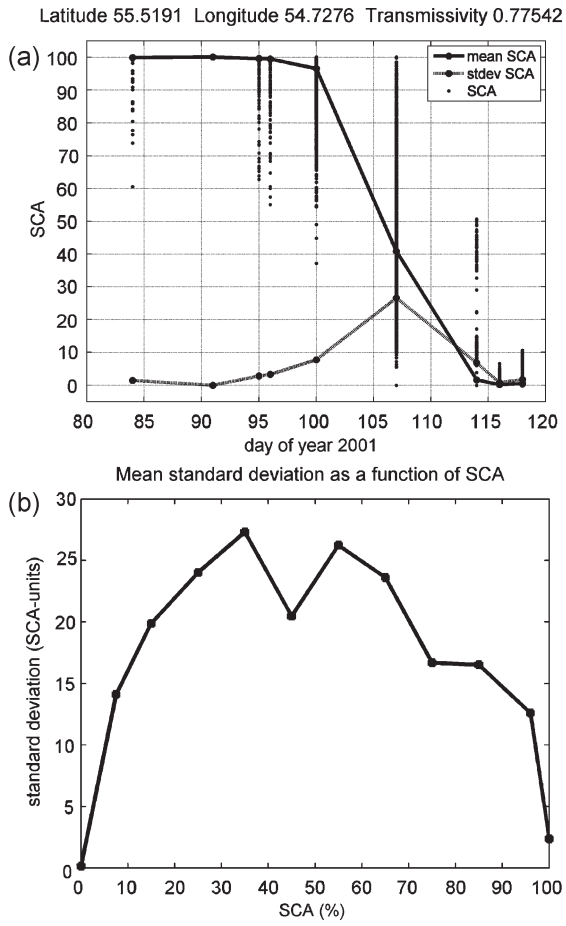

Fig. 4. Spatial variability of snow cover in 25 km × 25 km EASE-Grid cells during the snowmelt period. (a) Example for a single grid cell showing the variability of SCA within the area (all samples, and their mean and standard deviation observed for the 500 m × 500 m MODIS pixels within the EASE-Grid pixel. (b) Overall standard deviation as a function of SCA for all investigated 25 km × 25 km EASE-Grid pixels.

C. Channel Difference Algorithm

Takala *et al.* [8], [10] described a simple channel difference algorithm to estimate the snowmelt. The algorithm was modified [9] in order to avoid the dependence on ground-based observed physical temperature. In this paper, the modified version [9] is used. The algorithm detects the snowmelt situation when

$$(T_{37\mathrm{v}} - T_{19\mathrm{v}}) > -21\ \mathrm{K} \quad (1)$$

$$(T_{37\mathrm{h}} - T_{19\mathrm{v}}) < -10\ \mathrm{K}. \quad (2)$$

T denotes the brightness temperature and subindices the frequency and polarization of the radiometer. Frequencies of 19 and 37 GHz are available only on the SSM/I. With SMMR, the 19-GHz frequency is replaced with 18 GHz. According to a brightness temperature modeling by Pulliainen *et al.* [28], this

can induce an error of 1–2 K to the frequency difference, which affects the generation of time series based on various instruments. However, one should note that time series algorithms are much more insensitive to such an error since they operate with relative values (see Section V in the following).

Additionally, if, in a period of seven days before the given date, there are no dry snow estimations, the snowmelt onset estimate is discarded. The dry snow estimate is calculated using the algorithm developed by Hall *et al.* [5].

Chang *et al.* [29] determine SD by

$$\mathrm{SD} = 1.59(T_{19\mathrm{h}} - T_{37\mathrm{h}}). \tag{3}$$

If conditions

$$\mathrm{SD} > 80 \quad T_{37\mathrm{v}} < 250\ \mathrm{K} \quad T_{37\mathrm{h}} < 240\ \mathrm{K} \tag{4}$$

are met, data are classified as dry snow according to the method by Hall *et al.* [5].

D. Neural Network Algorithms

Supervised and unsupervised neural network structures were also tested to estimate the day of snowmelt.

Takala *et al.* [10] described a snowmelt detection algorithm based on SOM [30]. As with other snowmelt detection algorithms, the dependence on knowing the snow water equivalence or physical temperature as prior information is typically undesirable. Thus, in this paper, the SOM-based algorithm is simplified to be used only with brightness temperature data.

SOM consists of a layer of neurons, which usually form a 2-D grid. For each neuron, there is a weight vector $\mathbf{w}$, and all the neurons share the input vector $\mathbf{T}$. In this paper, the input vector is $\mathbf{T} = [T_{19\mathrm{v}}\ T_{22\mathrm{v}}\ T_{37\mathrm{v}}\ T_{19\mathrm{h}}\ T_{37\mathrm{h}}]$. The 22-GHz channel has no significant effect to the results and could be left out. The trained network normally operates as follows [31]. The input vector $\mathbf{T}$ is presented to every neuron in the network. All the neurons have a different weight vector $\mathbf{w}$, and the Euclidean distance of the weight and input vector for every neuron is calculated. The neuron whose weights are closest to the input is activated. This can be interpreted so that the input vector $\mathbf{T}$ presented to the network is classified to belong to the vector class of neuron k. SOM learns unsupervised, which means that it is unknown that a particular neuron responds to a certain class of input vectors.

The trained network is used by feeding the input vector and checking out which neuron is activated. After training, only such input vectors are selected, for which SD is less than 1 cm. The neuron winning in most cases is then selected to represent the case when snowmelt takes place. Typical for a SOM is that the classes presented by adjacent neurons in the fully trained network have more similar classification properties than that by distant neurons. This means that a group of neighboring neurons, instead of a single neuron, can represent the correct classification of snowmelt. In this paper, 3×3 neurons have been used.

The other tested method is the use of a feedforward neural network [31], a network whose neurons do not have any feedback from their output back to the input. Each neuron consists of a weight vector $\mathbf{w}$ and an input vector $\mathbf{x}$. There can be an additional bias term that always has a constant value of one and its own weight. The dot product between the input vector and the weight vector is calculated, and an activation function is applied to this value. An activation function can be linear or nonlinear. If the backpropagation algorithm is used, the activation must be differentiable. Commonly, a linear or sigmoidal function is used. The trained network is used as follows. First, all the outputs of the neurons in the hidden layer are calculated. Next, the outputs of the neuron(s) of the output layer are calculated. The signal propagates from the input layer to the hidden layer and then to the output layer. The output vector $\mathbf{y}$ corresponding to the input vector $\mathbf{x}$ is thus obtained.

Unlike SOM, a feedforward neural network learns supervised. Initially, the weights of every neuron are randomly assigned. The input vector $\mathbf{x}$ is presented to the network, and the output $\mathbf{y}'$ is calculated. For a supervised network, the desired output $\mathbf{y}$ is known. The error $\mathbf{y}' - \mathbf{y}$ is then calculated. The functional form of the activation function is known, as well as the current values of the weights. The relative amount of the error of each hidden-layer neuron can thus be propagated back from the output layer. The error is calculated backward until the input layer is reached. Since the error for each neuron is known, the weights are then adjusted such that the error gets smaller. The amount of adjusted weight is controlled with a learning parameter that gradually decays in time. Thus, it is ensured that the network reaches some state of equilibrium. This backpropagation of error and adjustment of weights are calculated for each pair of training input vector $\mathbf{x}$ and output vector $\mathbf{y}$. When the adjustments of the weights or the error of the output is reasonably small, the training is considered to be finished.

In this paper, the input vector $\mathbf{T} = [T_{19\mathrm{v}}\ T_{22\mathrm{v}}\ T_{37\mathrm{v}}\ T_{19\mathrm{h}}\ T_{37\mathrm{h}}]$ is the same as for the case of SOM (again, the 22-GHz channel can be left out). The feedforward network has an input layer, a hidden layer, and an output layer. The network consists of five neurons in the hidden layer and one neuron in the output layer. The activation function is sigmoid for all neurons. Other functional forms like tangent sigmoid and linear activation [31] were tested but discarded. The training output vector is determined as follows. If SD is less than 1 cm, the output is one; otherwise, the output is zero.

E. Time Series Thresholding Algorithm

The three previously presented algorithms attempt to determine the snowmelt on a daily basis. For the purpose of climatic analysis, the time series approach may be better suited. The channel difference $T_{37\mathrm{v}} - T_{19\mathrm{v}}$ is commonly used [4], [17] in passive microwave remote sensing of snow. A typical example of the time series of SD and the channel difference is shown in Fig. 2. As the snow melts and SD decreases, the channel difference increases. This observation leads to the following algorithm. Determine the maximum and minimum of the channel difference $T_{37\mathrm{v}} - T_{19\mathrm{v}}$, and when a certain level above the minimum is achieved, the snowmelt is considered to take place. This is shown as a detection limit in Fig. 2.

Sometimes, depending on location, the pointwise-observed snow status flag and the melt indices based on brightness temperature channel difference fluctuate considerably. Since the measurements of a radiometer are sensitive to the presence of liquid water, possibly, the observed fluctuation is related

to cyclic melting and freezing of the surface of the snowpack. However, in most cases, the difference between the final snowmelt and these temporary melt–refreeze cycles is distinguishable. Thus, the snowmelt is more accurately estimated from the maximum and minimum of the time average of the channel difference.

Thus, we obtain

$$D(t) = T_{37v}(t) - T_{19v}(t) \tag{5}$$

$$D_{\max,tavg} = \max\langle D(t_0), D(t_1), \ldots, D(t_N)\rangle \tag{6}$$

$$D_{\min,tavg} = \min\langle D(t_0), D(t_1), \ldots, D(t_N)\rangle \tag{7}$$

$$\langle D(t)\rangle \geq p \cdot [D_{\max,tavg} - D_{\min,tavg}] + D_{\min,tavg} \tag{8}$$

where D is the channel difference, t is the time (in days), and p is the level of detection (often 90%; $p = 0.9$). For each time t, condition (8) is evaluated. If it holds, the estimate for time t has a value of one; otherwise, it is zero.

The averaging period of seven to eight days gave the best results when many different averaging periods were tested. Since averaging determines only the detection limit, and detection is made from the original channel difference data, the spikes produced by temporary melt events are quite often detected. For some purposes, this is desirable. Typically, the most important melting incident is the actual snow clearance date. To determine that time, one must eliminate the temporary melts from the data. This can be satisfactorily achieved by averaging the estimate vector and thresholding at some level between zero and one (value of 0.9 found here). The threshold value of 0.9 was empirically determined to obtain a good fit.

III. Method Validation and Results

The validation is based on qualitative pointwise observations (INTAS-SSCONE snow flags), as described earlier. In Section II, we concluded that the pointwise nature of snow clearance data is not a problem when validating the radiometer-based estimates. In this investigation, snow status coding with more quantification levels than the INTAS-SSCONE data can offer is appreciated. In practice, this was only possible for the region of Finland, for which FMI weather station observations with detailed snow status information were available. Therefore, we compared the brightness temperature data with SD and snow status codes from FMI observations. The snow status code has values of nine for dry snow with 100% coverage, seven for wet snow with 100% coverage, six for wet snow with coverage $> 50\%$, and five for snow with coverage $< 50\%$. The temporary (value of two) and continuous melting (value of one) flags in the INTAS-SSCONE database correspond to the values that are greater than seven in the FMI weather observation data flag.

Fig. 2 shows an example of the FMI snow status code and SD in comparison to the brightness temperature channel difference. The detection limit of the algorithm described in Section II-E is also plotted. Fig. 2 shows that the qualitative estimate agrees relatively well with the observed changes in brightness temperature difference for this case. The observed difference between the regional satellite-databased estimate and observations at a single station is about five days. The SD measurements and flag estimates are made at a single location only. Uncertainties arise as the measurements in a single location

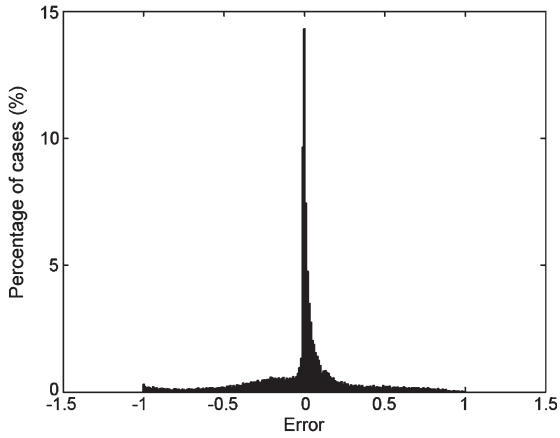

Fig. 5. Feedforward network was trained with input brightness temperature data and desired output data. The network was trained with ascending-node data and even years from 1990 to 2000. After the training, the input data set used in training was fed to the network, and an estimate of the output was calculated and compared to the desired output. If the training was successful, almost all the cases would have an error that was very close to zero.

are considered to represent to the area surrounding the station location and the area corresponding a whole EASE-Grid pixel. However, as Fig. 4 shows, point observations can be considered as good representatives of the SD and melt in the whole region. However, it should be kept in mind that the qualitative nature of the snow status flag is a potential source of error in accuracy assessments.

To test and compare the performance of the four algorithms, data from all 223 SD measurement sites were extracted for a period of 180 days beginning January 1 every year. Brightness temperature data from corresponding pixels of EASE-Grid were extracted as well. The SSM/I data were selected for testing. The years from 1990 to 2000 were used in the validation process. The purpose of validation is to compare the performance of different algorithms and not to address calibration issues between different instruments. Neural-network-based algorithms use part of the data for the training of the network. The SOM and feedforward network were trained with data from even years and validated with odd years or vice versa. Channel difference and time series thresholding algorithms do not need actual training data. However, the triggering value $p = 0.9$ was empirically selected for the time series algorithm (8), as that value gave the highest performance in algorithm testing.

Algorithms were validated with the data of odd or even years in order to enable comparison with other algorithms.

Tests were conducted for both ascending (afternoon) and descending (early morning) data. In the case of neural-network-based algorithms, a good weight set was selected from a set of ten different training runs. The quality of the training was determined visually by inspecting the error histogram. In the case of feedforward network, it is possible to compare how well the network learned to estimate the output data from the input data. This is shown in Fig. 5.

With time series thresholding, it became apparent that missing data, together with postfiltering, cause some detections to vanish, and this is problematic when maps of snowmelt are calculated. If the SMMR data are used, there are lots of data gaps due to the narrow swath width. Thus, interpolation

TABLE I
STATISTICAL ERROR CHARACTERISTICS OF DIFFERENT ALGORITHMS WITH DIFFERENT PARAMETERS VARIED DURING THE 1990–2000 TEST PERIOD

Algorithm	Mean (days)	Median (days)	Standard Deviation (days)	Node	Even or Odd Years
Channel	20.3	13	35.1	A	E
Difference	12.1	4	34.6	D	E
Algorithm	19.5	13	36.1	A	O
	14.8	6	36	D	O
SOM Neural	6.1	6	31.1	A	E
Network	23.9	20	39	D	E
Algorithm	-6.1	-8	32.1	A	O
	16.9	14	39.8	D	O
Feedforward	22.4	21	37.5	A	E
Neural	22.6	20	38.7	D	E
Network	-5.5	-8	35.4	A	O
Algorithm	-14.2	14	33.2	D	O
Time Series	-3.2	-2.5	16.9	A	E
Thresholding	-5.4	-5	15.3	D	E
Algorithm	-2.6	-3	18.3	A	O
	-7.7	-9	16.8	D	O
Time Series	1.6	1	21.5	A	E
Thresholding	-3.9	-4	21.2	D	E
with	2.1	0	22.3	A	O
Interpolation	-4.25	-4	21.3	D	O

A = ascending (afternoon data) D=descending (early morning data)

of channel difference data with time series thresholding was included in order to obtain a full spatial coverage.

The estimation error for a particular year at a particular test site is

$$\varepsilon = t_{\text{observed}} - t_{\text{estimated}}. \tag{9}$$

The unit of melt detection moment t is one day; t_{observed} refers to the INTAS-SSCONE-data-derived snow clearance date (according to the snow flag value), and $t_{\text{estimated}}$ refers to the estimated date of snowmelt using a particular algorithm. For each algorithm, the mean, median, and standard deviation of all the errors are calculated for a testing period of 1990–2000. If either observation or estimate is missing, the value is not taken into account. The results are presented in Table I. Four different sets of values are presented, depending whether ascending or descending data are used and whether the testing material has been taken from even or odd years. Results clearly suggest that time series thresholding is the most accurate algorithm in terms of mean (from -4.25 to 2.1 days) and standard deviation of estimation error (from 15.3 to 22.3 days), so this is the most applicable one among the tested algorithms for the purpose of climatic studies.

Since the comparison of different algorithms in Table I was carried out only using the SSM/I data, it was crucial to test the time series thresholding algorithm with the SMMR data in order to verify their similar behavior. Therefore, snowmelt day estimates using both SSM/I and SMMR data were calculated for as long periods as possible (both reference and satellite data available). Interpolation of missing brightness temperature values was used for both sensors. The results are shown in Fig. 6, showing a very good performance of snowmelt estimations with mean errors (biases) of only 0.6 and 1.1 days for the SMMR and SSM/I, respectively. Both SMMR and SSM/I data gave similar results with respect to the reference INTAS-SSCONE data, indicating that the joint use of these two sensors in long-term climate analyses is feasible.

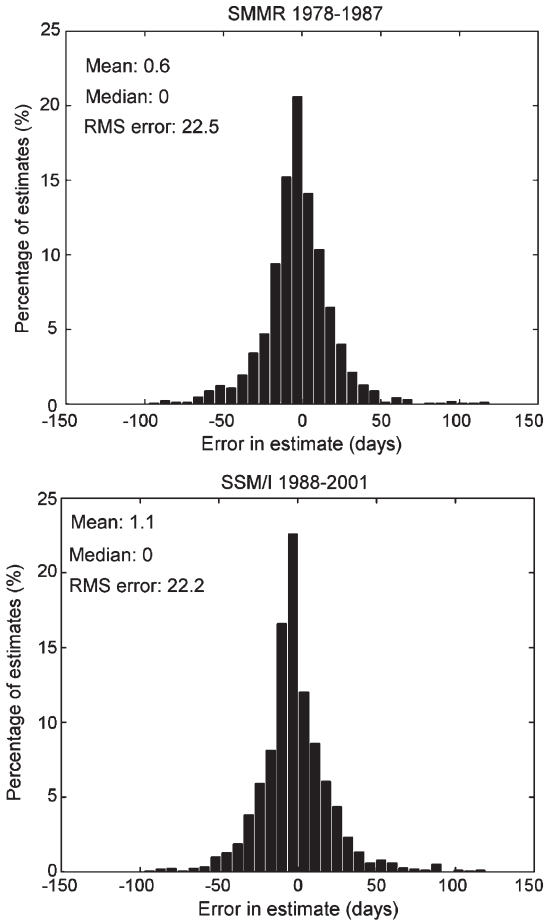

Fig. 6. Error distribution according to (9) of the time series thresholding algorithm (5)–(8), together with interpolation of lacking brightness temperature data. There are 1704 and 2205 applicable snow clearance estimates for the SMMR and SSM/I, respectively.

The performance of radiometer-databased snowmelt mapping is shown in Fig. 8. The calculated maps of the snowmelt in northern Eurasia for 1980, 1990, 2000, and 2007 clearly indicate how the melt is distributed geographically. The results also show interannual variations. For a few chosen test sites that are circular in shape with radius of 250 km and the center in Sodankylä, Verhoyansk, Tunguska, Novosibirsk, and Moscow, the time series of snowmelt estimates are shown in Fig. 7. The mean (averaged over time) snowmelt dates for these locations are the days of year 139, 146, 132, 113, and 100, respectively. The corresponding standard deviations in the timing of snowmelt are 6.7, 5.6, 9.1, 6.7, and 11.7 days. The slopes of the linear fits are -0.34, -0.24, -0.43, -0.07, and -0.69, respectively. The statistical significance was tested by calculating 95% and 90% confidence levels for the slope. The results are presented in Table II. Comparisons of the confidence intervals with slope 0 indicate that the trends are, in general, significant.

Detailed analysis of the difference between INTAS-SSCONE observations and radiometer-databased melt estimates, as a function of time, was also carried out. The results indicate that mean yearly bias can show values that are slightly different for the early years (SMMR data) than for the later period (SSM/I data). This would cause an effect of about -1.6 days

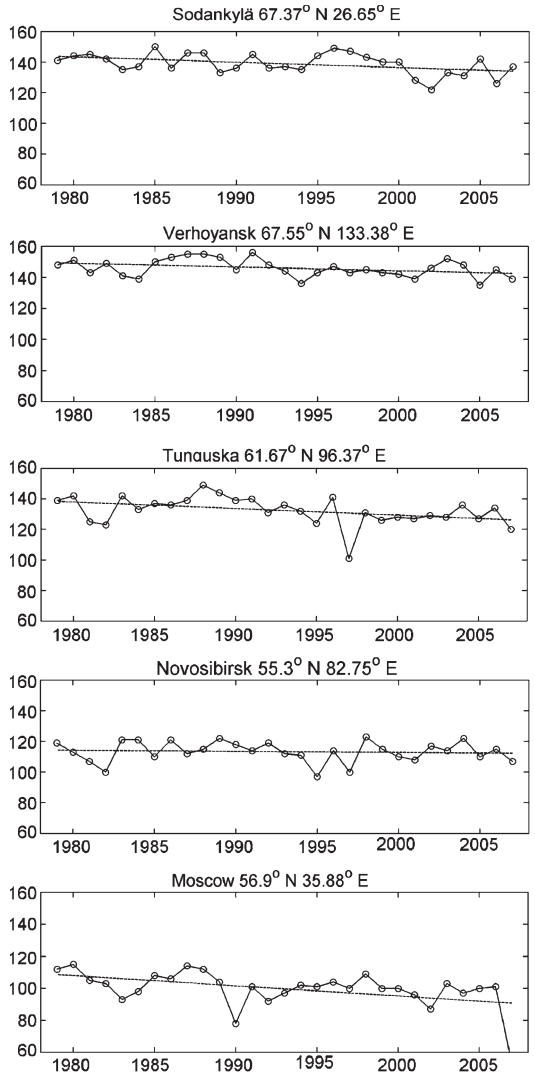

Fig. 7. Snowmelt in five different test sites in Eurasia on 1979–2007. The onset of snowmelt is averaged for a circular area having a radius of 250 km, and the place in the title is in the center of the area. The confidence levels of the slopes are presented in Table II.

TABLE II
SLOPES AND 90% AND 95% CONFIDENCE LEVELS CALCULATED FOR THE SLOPES IN FIG. 7

Centre of the circular test area with 250 km radius	Slope	95% lower bound	95% upper bound	90% lower bound	90% upper bound
Sodankylä	-0.35	0.64	-0.06	-0.59	-0.11
Verhoyansk	0.24	-0.49	0.00	-0.45	-0.04
Tunguska	-0.43	-0.83	-0.04	-0.76	-0.10
Novosibirsk	-0.07	-0.39	0.24	-0.33	0.19
Moscow	-0.64	-1.13	-0.15	-1.05	-0.23

per decade for the estimated trend of snowmelt. In practice, the analysis suggests that a value of 2.6 days should be added to the snowmelt dates representing years 1979–1987, resulting to slightly delayed snow clearance dates. Moreover, a value of 1.0 day should be subtracted starting from the year 1992 indicating earlier snowmelt dates than those shown in Fig. 7. Thus, if this correction is made, the negative trends shown in Table II and Fig. 7 would magnify (a decrease of 0.16 to slope factors in Table II). For 1988–1991, the analysis of temporal bias indicates a mismatch between INTAS-SSCONE snowmelt dates and radiometer retrievals higher than that obtained for other 19 years. This may indicate problems in either reference or satellite data (first SSM/I instrument onboard the F08 satellite).

The slope of the linear fit was calculated for every pixel in Eurasia [Fig. 9, (top)] to demonstrate the evolution of snow clearance date in the period of 29 years. Red tones with negative values indicate earlier melt, whereas blue tones with positive values indicate later melt. The corresponding slopes were also calculated using the station-wise data from INTAS-SSCONE stations [Fig. 9, (bottom)]. Fig. 9 (top) is determined by including the bias correction between the SMMR and SSM/I data retrievals discussed earlier. However, this has only a marginal effect to the results (it decreases the shown trend with a constant −1.6 days/decade). Years 1988–1991 were excluded from the trend analysis of Fig. 9 (top).

IV. DISCUSSION

The comparison of different algorithms in Table I reveals immediately one important aspect. When channel difference and neural-network-based algorithms are used, the standard deviation between the estimated snow clearance date and the reference data is as high as over 30 days, but when time-series-analysis-based algorithms are used, the standard deviation reduces to slightly above 20 or even less. This is explained by the fact that the first three mentioned algorithms examine the data on a daily basis with only current and historical observations available, whereas the time series algorithm takes the whole time series of radiometer observations into account. This justifies the offline use of time-series-based algorithms when accuracy is the main concern, such as in historical climate studies. However, in operational (near real time) use, data can only be analyzed using current day or past observations. An important factor contributing to the error distribution is the accuracy of estimation of the snowmelt date from the snow status flag. The flag is a qualitative estimate and can thus be inaccurate.

The channel difference algorithm (1)–(4) has a standard deviation that is close to 35 days, regardless if even or odd years are used or whether the data used are either from ascending or descending node. It is evident that the selection of orbital node affects the mean and median. This can be explained by the local time that is either early morning or late afternoon. The diurnal melting cycle during the day causes the signatures to be different and, hence, the difference in mean. The clear difference between median and mean indicates an asymmetric deviation of error. Since the algorithm was originally developed using snow wetness data from hydrological model predictions only, it is possible that the asymmetry is due to the different kinds of data applied for algorithm development.

The self-organizing network-based algorithm seems to work better when trained and tested with ascending-node data. Both mean and median errors are closer to zero when using ascending node instead of observations from descending node.

Switching between even and odd years does not seem to affect the quality of the algorithm. The error distribution is more symmetric than in the case of the channel difference algorithm. Although the SOM-based algorithm seems to work, it does not offer any significant advantage over the much simpler channel difference algorithm.

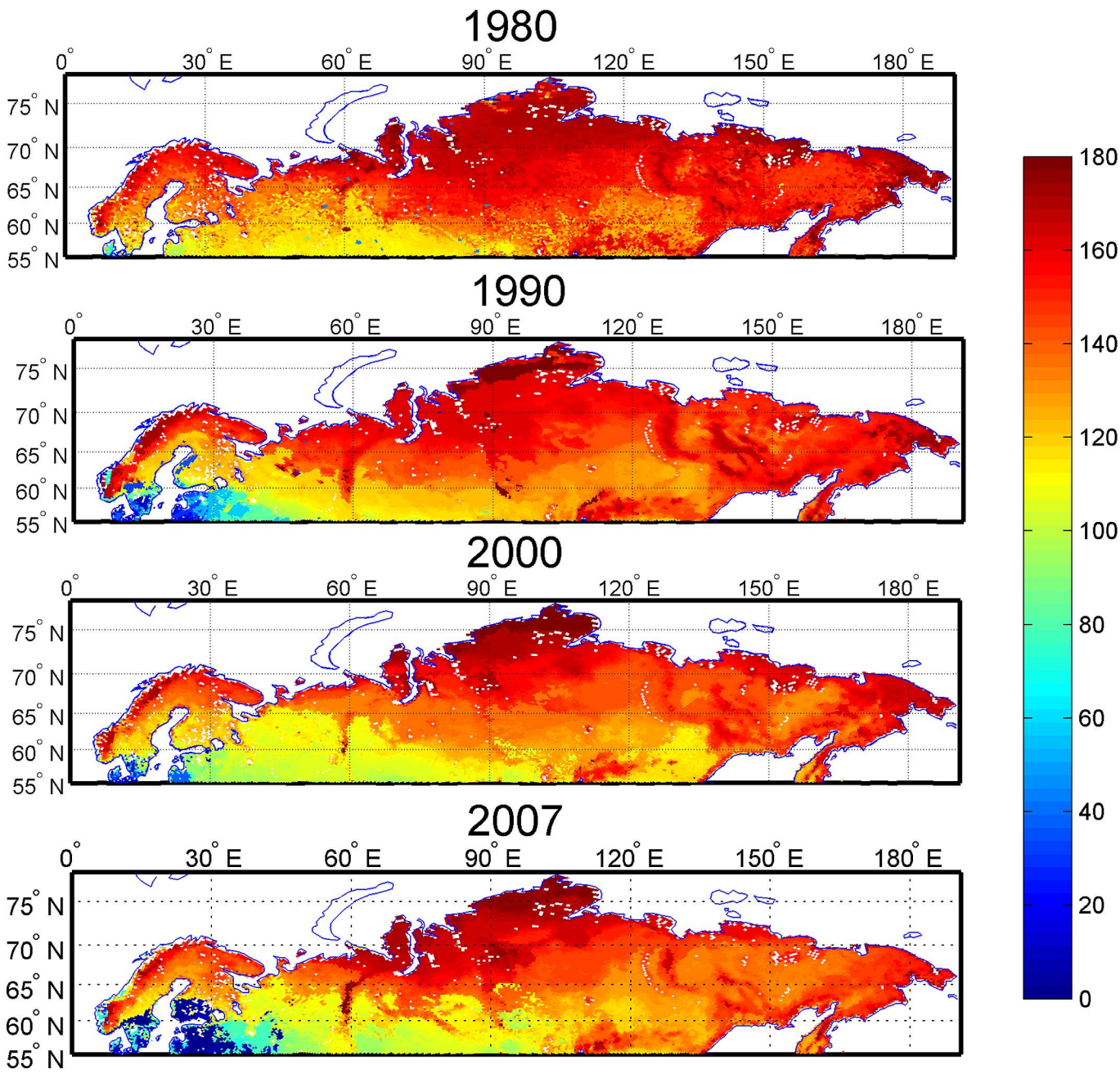

Fig. 8. Maps of the onset of snowmelt for 1980, 1990, 2000, and 2007. The results are calculated using the time series thresholding algorithm. The color code is the number of days since January 1 corresponding year.

The standard deviation using the feedforward neural-network-based algorithm seems to be slightly lower when tested with data from odd years. Mean and median errors tend to be closer to zero also when data are from odd years. The distribution of error is quite symmetric. Again, no significant advantage over the simpler algorithm is seen. Since the feedforward algorithm is trained supervised, it is possible to check how well the neural network can be trained (Fig. 5). If a supervised neural network is perfectly trained, the output error is very close to zero when the network is fed with an input vector used in the training.

After a particular training feeding, the network with input vectors used in training ends up with about 50% of the cases that are close to zero and about 50% that are not. This suggests that the differentiation between snow-covered area and bare ground is sometimes possible and sometimes not. This is logical since very wet snow and bare wet ground contain liquid water, and the microwave emissivity can be close to one in both cases. Although different training sessions and varying training parameters have been applied, the result can be a consequence of improper training. To overcome this problem, additional data, such as temperature data derived from synoptic stations or infrared satellite observations, could be used.

The time series thresholding algorithm (5)–(8) without channel data interpolation performs better when descending-node (early morning) data are used. However, the mean and median

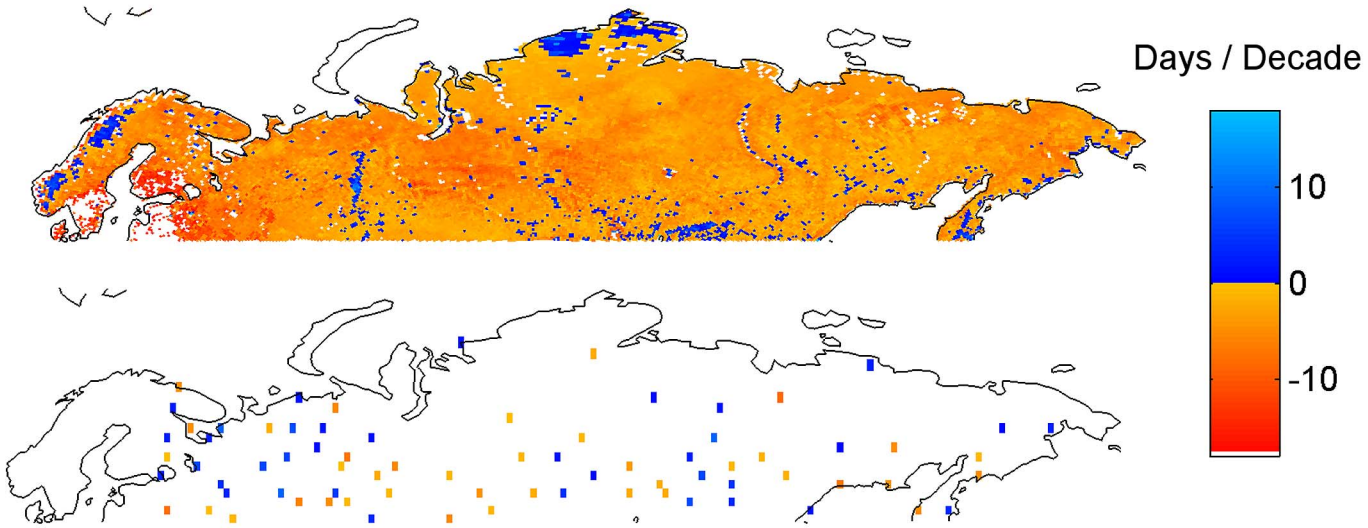

Fig. 9. Change in snow clearance date per decade estimated applying (top) the channel difference algorithm to satellite data and derived from (bottom) INTAS-SSCONE test sites. The red tones and negative values mean earlier melt, and the blue tones and positive values mean later melt. The numerical value is days per decade.

are closer to zero when ascending data are used. The use of even or odd years does not affect the results. By plotting the maps, it became evident that some cases in error analysis were discarded due to the missing data. When channel difference data are interpolated for the missing dates, the results become somewhat different. The standard deviation is larger than in the case of noninterpolated channel data, but this could be easily explained as the error contribution from missing data cases is discarded in postprocessing. The error then does not depend on the node or the years used. Using ascending data, the mean and median are very near to zero.

Since gaps are typical with SMMR observations, the error analysis was extended to the SMMR data using channel data interpolation for years 1979–1987. The same procedure was conducted for the SSM/I data for every year from 1988 to 2001. Fig. 6 shows that the mean, median, and standard deviation are almost the same for both instruments. As presented in Section II-B, the pointwise measurement of SD represents the 25 km $\times$ 25 km EASE-Grid pixels when the snow cover is full or almost melted.

In Fig. 8, the snowmelt for the whole Eurasia is shown for 1980, 1990, 2000, and 2007. Although there is variation between years, the maps feature a different development of snowmelt in Europe when compared with Asia. Very early snowmelt dates obtained for the southwest part of the map region indicate that the actual seasonal (permanent) snow cover does not typically exist for this part of Europe. This overall behavior is most probably due to the effect of Arctic oscillation [23], [25] and North Atlantic oscillation [23]. Some geographical features, such as Scandinavian mountains and Ural, are visible since the snow begins to melt later on the high mountains. The effects of topography and land use affect the microwave brightness temperature. Recently, many global land use maps have become available, but their usefulness in analysis is limited [32], [33]. This is somewhat true for local land cover data too [34]. The authors will address this problem in a more detailed manner in future work.

In Fig. 6, the temporal behavior of the snowmelt for some locations in Eurasia is presented. The negative slopes indicate that the snow now melts 1–7 days earlier than it did ten years ago.

The 95% and 90% confidence intervals for the slopes are presented in Table II. The negative trend is a statistically significant trend in most cases. The geographic location of the test site is significant. The more to the south and the more to the west the location is, the earlier the snowmelt is. The largest negative slope value around Moscow indicates that the change in snowmelt in the European side of Eurasia has been more rapid than in the Asian side. The results are, in general, in line with the analyses performed by Dye [24] and Smith *et al.* [13].

In Fig. 9 (top), the decadal trend map of snow clearance date derived from satellite data demonstrates that the snow melts earlier today than it did 29 years ago in most parts of Eurasia, particularly in the European side of Eurasia. On mountains such as Ural and Scandinavia, on some wetlands, and on large areas of Arctic tundra, the melt appears to take place later in recent years. This can either be a real phenomenon caused, for example, by increased snow fall or an anomaly due to land cover and/or topography, which needs to be researched further. For applicable INTAS-SSCONE stations, the trend map has been derived [Fig. 9, (bottom)]. These results do not show such clear spatial trends as the satellite-data-derived map do [Fig. 9, (top)]. A possible reason is that the available pointwise observations may exhibit a higher variance with respect to the real timing of snowmelt than the satellite data retrievals (as areal melting characteristics for grid cells of 25 km $\times$ 25 km are considered here). Additionally, the spatial distribution of INTAS-SSCONE monitoring stations is sparse. Thus, ground-based observations cannot be interpolated to yield the trend map derived from satellite data, even though they can be used to calibrate and validate satellite-databased snow clearance date estimates. An important finding is that the mean annual difference between pointwise INTAS-SSCONE reference data and satellite data retrievals only shows a slight difference between SMMR and SSM/I data retrievals but not otherwise. The difference between the sensors

can be accounted for in trend analysis, which is performed in Fig. 9. The magnitude of this correction for the decadal trend is -1.6 (days per decade). The results of Fig. 9 (top) only slightly change if this correction factor is excluded. It can be concluded that the satellite-data-derived snowmelt trend shown in Fig. 9 (top) is a realistic estimate; the level of error cannot, in general, exceed the value of about 1.6 days per decade.

In the case of real-time operational use, the time series algorithm cannot be used as such since it requires the brightness temperatures to be available for the period when the snowmelt had already taken place. The performance of channel difference and neural network algorithms are not at the same level with that of the time series algorithm. However, the error estimates are based on comparisons with point observations, and the accuracy characteristics over larger areas may be higher than the quantitative values reported here.

The accuracy of snow clearance date estimates could be possibly improved by applying in future work *in situ* data as supplementary data to radiometer observations. The effect of land use must also be addressed. Land use classification GLC2000 [35] suggests that the land use of the Tunguska site is "water bodies." This partly explains the largest value of standard deviation of snowmelt in Fig. 6. Although the time series approach is much better in terms of accuracy, the effect of land use may be present.

V. Conclusion

This paper has shown that it is possible to estimate snowmelt dates accurately in Eurasia from spaceborne microwave brightness temperature data. The results showed a standard deviation of $\sim$20 days when compared with pointwise reference *in situ* data. MODIS-databased analysis showed that the pointwise observation was a valid representation for the 25 km $\times$ 25 km pixels at the time of snow clearance, and thus, the INTAS-SSCONE data can be used as reference data for satellite observations. Altogether, four algorithms to map snowmelt were proposed and tested. The best agreement with reference data was obtained using the time series thresholding algorithm.

Snowmelt maps were derived and analyzed for 29 separate years from 1979 to 2007. The melting trend had been mapped for the whole Eurasia, and the results showed that snow melted earlier in the European part of Eurasia than in the Asian part. Examples for a few chosen locations around the area show statistically significant negative trends indicating that snow melted even a month earlier than it did 29 years ago. The results also suggested that interpolating the trend from pointwise observation was not feasible, whereas satellite observations provided such information.

References

[1] L. C. Shaffrey, I. G. Stevens, W. A. Norton, M. J. Roberts, P. L. Vidale, J. D. Harle, A. Jrrar, D. P. Stevens, M. J. Woodage, M. E. Demory, J. Donners, D. B. Clark, A. Clayton, J. W. Cole, J. C. King, A. L. New, J. M. Slingo, A. Slingo, L. Steenman-Clark, and G. M. Martin, "UK-HiGEM: The new UK high resolution global environment model. Model description and basic evaluation," *J. Climate*, vol. 22, pp. 1861–1896, 2009, doi:10.1175/2008JCLI2508.1.

[2] J. Martinec and K. Seidel, "Remote sensing in snow hydrology; Runoff modelling," in *Effect of Climate Change*. New York: Springer-Verlag, 2004.

[3] W. Abdalati and K. Steffen, "Passive microwave-derived snow melt regions on the Greenland ice sheet," *Geophys. Res. Lett.*, vol. 22, no. 7, pp. 787–790, 1995.

[4] S. D. Drobot and M. R. Anderson, "An improved method for determining snowmelt onset dates over Arctic sea ice using Scanning Multichannel Microwave Radiometer and Special Sensor Microwave/Imager data," *J. Geophys. Res.*, vol. 106, no. D20, pp. 24 033–24 049, 2001.

[5] D. K. Hall, R. E. J. Kelly, G. A. Riggs, A. T. C. Chang, and J. L. Foster, "Assessment of the relative accuracy of hemispheric-scale snow-cover maps," *Ann. Glaciol.*, vol. 34, pp. 24–30, 2002.

[6] M. Joshi, C. J. Merry, K. C. Jezek, and J. F. Bolzan, "An edge detection technique to estimate melt duration, season and melt extent on the Greenland ice sheet using passive microwave data," *Geophys. Res. Lett.*, vol. 28, no. 18, pp. 3497–3500, 2001.

[7] N. M. Mognard, A. V. Kouraev, and E. G. Josberger, "Global snow-cover evolution from twenty years of satellite passive microwave data," in *Proc. IEEE IGARSS*, Toulouse, France, Jul. 21–25, 2003, pp. 2838–2840.

[8] M. Takala, J. Pulliainen, M. Huttunen, and M. Hallikainen, "Estimation of the beginning of snow melt period using SSM/I data," in *Proc. IEEE IGARSS*, Toulouse, France, Jul. 21–25, 2003, pp. 2841–2843.

[9] M. Takala, J. Pulliainen, and P. Lahtinen, "Estimating the snow melt onset using AMSR-E data in Eurasia," in *Proc. IGARSS*, Barcelona, Spain, Jul. 23–27, 2007, pp. 4221–4224.

[10] M. Takala, J. Pulliainen, M. Huttunen, and M. Hallikainen, "Detecting the onset of snow-melt using SSM/I data and the self-organizing map," *Int. J. Remote Sens.*, vol. 29, no. 3/4, pp. 755–766, Feb. 2008.

[11] S. P. Anderton, S. M. White, and B. Alvera, "Micro-scale spatial variability and the timing of snow melt runoff in a high mountain catchment," *J. Hydrol.*, vol. 268, no. 1–4, pp. 158–176, Nov. 2002.

[12] M. Grippa, L. Kergoat, T. Le Toan, N. M. Mognard, N. Delbart, J. L'Hermitte, and S. Vincente Serrano, "Impact of snow depth and snowmelt on vegetation activity in Siberia: A 12 years study using remote sensing data from SSM/I and AVHRR," *Geophys. Res. Abstr.*, vol. 7, p. 08 048, 2005.

[13] N. V. Smith, S. S. Saatchi, and J. T. Randerson, "Trends in northern latitude soil freeze and thaw cycles from 1988 to 2002," *J. Geophys. Res.*, vol. 109, no. D12, p. D12 101, 2004.

[14] R. L. Armstrong, K. W. Knowles, M. J. Brodzik, and M. A. Hardman, *DMSP SSM/I Pathfinder Daily EASE-Grid Brightness Temperatures, Jan. 1987–Jul. 2007*. Boulder, CO: Nat. Snow Ice Data Center. Digital Media, 1994.

[15] K. Knowles, E. Njoku, R. Armstrong, and M. J. Brodzik, *Nimbus-7 SMMR Pathfinder Daily EASE-Grid Brightness Temperatures*. Boulder, CO: Nat. Snow Ice Data Center, 2002. Digital Media and CD-ROM.

[16] D. K. Hall, R. S. Williams, K. Steffen, and J. Y. L. Chien, "Analysis of summer 2002 melt extent on the Greenland sheet using MODIS and SSM/I data," in *Proc. IEEE IGARSS*, Anchorage, AK, Sep. 20–24, 2004, pp. 3029–3032.

[17] D. M. Smith, "Observation of perennial Arctic sea ice melt and freeze-up using passive microwave data," *J. Geophys. Res.*, vol. 103, no. C12, pp. 27 753–27 769, 1998.

[18] M. Tedesco, J. Pulliainen, M. Takala, M. Hallikainen, and P. Pampaloni, "Artificial neural network-based techniques for the retrieval of SWE and snow depth from SSM/I," *Remote Sens. Environ.*, vol. 90, no. 1, pp. 76–85, Mar. 2004.

[19] J. J. Simpson and T. J. McIntire, "A recurrent neural network classifier for improved retrievals of areal extent of snow cover," *IEEE Trans. Geosci. Remote Sens.*, vol. 39, no. 10, pp. 2135–2147, Oct. 2001.

[20] J. L. Foster, J. W. Winchester, and E. G. Dutton, "The data of snow disappearance on the Arctic tundra as determined from satellite meteorological station and radiometric *in situ* observations," *IEEE Trans. Geosci. Remote Sens.*, vol. 30, no. 4, pp. 793–798, Jul. 1992.

[21] L. Kitaev, A. Kislov, A. Krenke, V. Razuvaev, R. Martuganov, and I. Konstantinov, "The snow characteristics of northern Eurasia and their relationship to climatic parameters," *Boreal Environm. Res.*, vol. 7, pp. 437–445, 2002.

[22] R. D. Brown, "Northern hemisphere snow cover variability and change, 1915–1997," *J. Clim.*, vol. 13, no. 13, pp. 2339–2355, Jul. 2000.

[23] M. C. Serreze, J. E. Walsh, F. S. Chapin, III, T. Osterkamp, M. Dyurgerov, V. Romanovsky, W. C. Oechel, J. Morison, T. Zhang, and R. G. Barry, "Observational evidences of recent change in the northern high-latitude environment," *Clim. Change*, vol. 46, no. 1/2, pp. 159–207, Jul. 2000.

[24] D. G. Dye, "Variability and trends in the annual snow-cover cycle in Northern Hemisphere land areas," *Hydrol. Process.*, vol. 16, no. 15, pp. 3065–3077, Oct. 2002.

[25] A. S. Bamzai, "Relationship between snow cover variability and arctic oscillation index on a hierarchy of time scales," *Int. J. Climatol.*, vol. 23, no. 2, pp. 131–142, Feb. 2003.
[26] J. Foster, D. Robinson, D. Hall, and T. Estilow, "Spring snow melt timing and changes over Arctic lands," *Polar Geogr.*, vol. 31, no. 3/4, pp. 145–157, Jan. 2008.
[27] S. Metsämäki, S. T. Anttila, J. M. Huttunen, and J. A. Vepsäläinen, "A feasible method for fractional snow cover mapping in boreal zone based on a reflectance model," *Remote Sens. Environ.*, vol. 95, no. 1, pp. 77–95, Mar. 2005.
[28] J. Pulliainen, J. Grandell, and M. Hallikainen, "HUT snow emission model and its applicability to snow water equivalent retrieval," *IEEE Trans. Geosci. Remote Sens.*, vol. 37, no. 3, pp. 1378–1390, May 1999.
[29] A. T. C. Chang, J. L. Foster, and D. K. Hall, "Nimbus-7 SMMR derived global snow cover parameters," *Ann. Glaciol.*, vol. 9, pp. 39–44, 1987.
[30] T. Kohonen, "Self-organized formation of topologically correct feature maps," *Biol. Cybern.*, vol. 43, no. 1, pp. 59–69, Jan. 1982.
[31] S. Haykin, *Neural Networks, A Comprehensive Foundation*, 2nd ed. Englewood Cliffs, NJ: Prentice–Hall, 1999.
[32] I. McCallum, M. Obersteiner, S. Nilsson, and A. Shvidenko, "A spatial comparison of four satellite derived 1 km global land cover datasets," *Int. J. Appl. Earth Obs. Geoinf.*, vol. 8, no. 4, pp. 246–255, Dec. 2006.
[33] M. Herold, C. Woodcock, P. Mayaux, A. Baccini, and C. Schmullius, "Some challenges in global land cover mapping," *Remote Sens. Environ.*, vol. 112, no. 5, pp. 2538–2556, May 2008.
[34] K. E. Frey and L. C. Smith, "How well do we know northern land cover? Comparison of four global vegetation and wetland products with a new ground-truth database for West Siberia," *Glob. Biogeochem. Cycles*, vol. 21, p. GB1 016, 2007. DOI: 10.1029/2006GB002706.
[35] *The Global Land Cover Map for the Year 2000. GLC2000 Database*, European Commision Joint Research Centre. [Online]. Available: http://bioval.jrc.ec.europa.eu/products/glc2000/glc2000.php

Matias Takala received the M.Sc. degree in technology from the Helsinki University of Technology (TKK), Espoo, Finland, in 2001.

From 2001 to 2006, he was a Research Scientist with TKK and has been a Research Scientist with the Finnish Meteorological Institute, Helsinki, since 2007. His research interests include microwave remote sensing of snow cover and developing remote sensing applications.

Jouni Pulliainen (S'91–M'95–SM'03) received the M.Sc., Lic.Tech., and Dr.Sc. (Tech.) degrees from the Helsinki University of Technology (TKK), Espoo, Finland, in 1988, 1991, and 1994, respectively.

From 1993 to 1994, he was the Acting Director of the Laboratory of Space Technology, TKK. From 2001 to 2006, he was a Professor of space technology with TKK, where he specialized in remote sensing. He is currently a Research Professor with the Finnish Meteorological Institute (FMI), Helsinki, Finland, where he is also the Head of the Arctic Research Centre. Recently, his work has focused on the active and passive remote sensing of boreal forests and snow cover applying both microwave and optical data (including atmospheric correction). He has been the Principal Investigator or Project Manger for several nationally funded and international research projects, including several ESA and EC contracts. His research interests include direct and inverse modeling in remote sensing and, additionally, remote sensing data assimilation and application development e.g., for the needs of climate change investigations. He has authored about 250 scientific papers and technical reports in the field of remote sensing.

Dr. Pulliainen was a member of the ESA Advisory Committee on Education (2001–2007). He is also a member of the ESA CoreH2O MAG (2007 onward) and the ESF European Space Sciences Committee (2008 onward).

Sari J. Metsämäki was born in Helsinki, Finland, in 1965. She received the M.Sc. degree from the Helsinki University of Technology, Espoo, Finland, in 1991.

Since then, she has been a Remote Sensing Scientist with the Geoinformatics and Land Use Division, Finnish Environment Institute, Helsinki. Her major scientific interest includes optical remote sensing of snow, particularly related to hydrological modeling. She is currently focusing on running and developing the Baltic Sea Area snow cover monitoring service under the Polar View program of the ESA/EU GMES initiative.

Jarkko T. Koskinen (S'96–A'98–M'02) received the Dr.Sc. (Tech.) degree from the Helsinki University of Technology (TKK), Espoo, Finland.

He is currently a Research Professor with the Finnish Meteorological Institute (FMI), Helsinki, Finland. He was with TKK, with SYKE as a Research Scientist, and with Tekes, where his responsibility was the coordination of the national Earth observation program. He worked twice abroad in 1994–1995 as a Young Graduate Trainee with ESA-ESRIN and in 1999–2000 as a Visiting Scientist with the NASA Jet Propulsion Laboratory. His research interests include microwave remote sensing of snow and boreal forest and synthetic aperture radar interferometry. He has authored over 80 scientific papers.

Prof. Koskinen holds several international positions of trust. He is delegate to ESA's Programme Board on Earth Observation, EUMETSAT's Policy Advisory Committee, the E.U.'s High Level GMES Advisory Council, and the Group on Earth Observation (GEO). He is also a member of the National Space Council. He was the Chairman of ESA's Data Operations Scientific and Technical Advisory Group in 2003–2005. He has also acted as Reviewer of several international journals and conferences.